Estuarine processes modify the isotope composition of dissolved riverine barium fluxes to the ocean

Luke Bridgestock[1]*, Joseph Nathan[1], Robert Paver[1], Yu-Te Hsieh[1], Don Porcelli[1], Jani Tanzil[2,3], Phil Holdship[1], Gonzalo Carrasco[2], Kogila Vani Annammala[4,5], Peter W. Swarzenski[6] and Gideon M. Henderson[1]

[1]Department of Earth Sciences, University of Oxford, South Parks Road, Oxford, OX1 3AN, UK

[2] Tropical Marine Science Institute, National University of Singapore, Singapore

[3] St. John's Island National Marine Laboratory, National University of Singapore, Singapore

[4] Centre of Environmental Sustainability & Water Security (IPASA), Research Institute for Sustainable Environment (RISE), Universiti Teknologi Malaysia, Johor, Malaysia

[5] Department of Water and Environmental Engineering, School of Civil Engineering, Universiti Teknologi Malaysia, Johor, Malaysia.

[6]International Atomic Energy Agency, Environment Laboratories, 98000, Monaco

*Corresponding author; ljb212@cam.ac.uk

Present address (Luke Bridgestock): Department of Earth Sciences, University of Cambridge, Downing Street, Cambridge, CB2 3EQ, UK

Keywords: Ba isotopes; estuaries; riverine Ba fluxes; marine Ba cycle;

Abstract; 281

Main text; 5935 words

Highlights

- Net global river Ba flux to the ocean estimated to be ~10 to 20 Gmol yr^{-1}
- Estuarine Ba release likely accounts for ~20-75% of this flux
- $\delta^{138/134}$Ba of net riverine inputs to ocean modified by estuarine Ba desorption
- Accounting for this process helps to balance the marine Ba isotope budget
- Adsorption to river particles fractionates Ba isotopes by 0.2 to 0.3 ‰

Abstract

Barium (Ba) isotope variations offer the potential to trace environmental processes, including long-term changes in river discharge and marine export production. Riverine inputs are an important source of dissolved Ba to the ocean, which we estimate to be ~10 to 20 Gmol yr^{-1}. A large fraction (~20 to 75%) of this net riverine dissolved Ba flux to the ocean is derived from estuarine processes, in particular the release of exchangeable Ba from riverine suspended particles due to exchange with major cations in seawater. Despite the importance of this process for controlling the input of dissolved Ba to the ocean, its impact on the $\delta^{138/134}$Ba of net riverine dissolved Ba fluxes remains unknown. To address this observational gap, Ba concentration and isotope data from across the estuarine mixing zones of the Amazon (Brazil), Fly (Papua New Guinea) and Johor (Malaysia) Rivers are presented. Desorption from suspended riverine particles releases Ba with $\delta^{138/134}$Ba 0.2 to 0.3 ‰ lower than corresponding river dissolved loads, modifying the isotope composition of net riverine dissolved Ba fluxes that reach the ocean. This offset likely represents an isotope fractionation accompanying the adsorption of Ba by particulate phases within river catchments, which can explain the systematic enrichment of heavier Ba isotopes in river dissolved loads relative to weathering lithologies. River dissolved loads are also systematically offset to higher $\delta^{138/134}$Ba than the main oceanic Ba sink: burial of $BaSO_4$

in marine sediment. This represents an apparent imbalance in the modern marine Ba isotope budget. Our results suggest that accounting for modification of the $\delta^{138/134}$Ba of net riverine Ba fluxes to the ocean by estuarine processes is likely to play a key role towards balancing the modern marine Ba isotope budget.

1. Introduction

The marine barium (Ba) cycle forms the basis of numerous approaches to trace environmental processes, including river discharge to the ocean (e.g. Fleitmann et al., 2007, Gebregiorgis et al., 2016) and past changes in marine export production (e.g. Paytan and Griffiths, 2007). Rivers are considered to be the dominant source of dissolved Ba to the ocean (Wolgemuth & Broecker, 1970, Paytan and Kastner, 1996), with estuarine processes playing a key role in controlling net riverine dissolved Ba fluxes to coastal waters (e.g. Coffey et al., 1997). A fraction of the Ba leached from mineral phases during chemical weathering is adsorbed onto the surfaces of secondary minerals within river catchments (Nesbitt et al., 1980, Price et al., 1991, Zhang et al., 2007, Gong et al., 2019, Gou et al., 2020). Upon the transport of this material through estuaries, this adsorbed Ba is released back into solution due to exchange with major cations in seawater (e.g. Hanor and Chan, 1977). This significantly enhances the dissolved Ba flux to coastal waters within most estuaries and creates interesting links between chemical weathering and physical erosion for controlling net riverine dissolved Ba fluxes to the ocean (e.g. McCulloch et al., 2003).

Stable Ba isotope variations are a new tool for studying the global biogeochemical cycle of this element. Initial observations indicate that river dissolved loads are enriched in heavier Ba isotopes relative to the major oceanic Ba sink, burial of $BaSO_4$ in marine

sediment (Crockford et al., 2019, Gou and Deng, 2019, Gou et al., 2020, Cao et al., 2020, Tieman et al., 2020). Marine Ba inputs from submarine groundwater discharge (Mayfield et al., 2021) and hydrothermal vents (Hsieh et al., 2021) are also enriched in heavier isotopes relative to this sink, representing an apparent imbalance in the modern marine Ba isotope budget (Horner and Crockford, 2021). Available data also show that river dissolved loads are generally enriched in heavier Ba isotopes relative to rocks (Nan et al., 2018, Gou and Deng, 2019, Gou et al., 2020, Cao et al., 2020, Tieman et al., 2020, Charbonnier et al. 2020). This difference is suggested to reflect the preferential adsorption of lighter Ba isotopes to mineral surfaces within soils (Gong et al., 2019, 2020) and riverine suspended sediment loads (Gou et al., 2020). Other processes such as Ba uptake into terrestrial biomass (Bullen and Chadwick, 2016) or secondary minerals (Gou et al., 2020), or isotope fractionation during leaching of Ba from primary minerals (Gong et al., 2020), could also play important roles in controlling the isotope composition of riverine Ba fluxes. These initial observations highlight the potential of Ba isotopes to trace these processes (e.g. Charbonnier et al., 2020), but improved understanding of the controls on riverine Ba isotope fluxes are still needed.

The cycling of Ba isotopes in estuaries represents a key observational gap in our understanding of the global Ba isotope cycle. Given the postulated isotope fractionation accompanying Ba adsorption to mineral phases within river catchments (Gou et al., 2020, Gong et al., 2019, 2020), the release of this Ba in estuaries due to cation exchange (e.g. Hanor and Chan, 1977) is likely to influence the isotope composition of net riverine Ba inputs to the ocean. Studying the cycling of Ba isotopes in estuaries is therefore required to help balance the modern marine Ba isotope budget and may provide insights into the role of adsorption for controlling the Ba isotope composition of riverine dissolved loads. To this end, this study presents dissolved Ba concentration and isotope data for transects

across the estuarine mixing zones of the Amazon, Fly and Johor Rivers. These estuaries were selected based on the availability of water samples obtained during previous sampling campaigns (Swarzenski et al., 2004, Chen et al., 2015). Unfortunately particulate samples were not available for these sample sets, nor were time-series samples to assess seasonal variations in net riverine Ba fluxes. Nevertheless, these sample sets are well suited to address the aims of this study, which are to gain first-order insights into role of particulate Ba release in estuaries for controlling the net riverine flux of Ba isotopes to the ocean.

2. Study area and samples

The Amazon River provides the largest freshwater (6300 km^3 yr^{-1}) and sediment (1200 Mt yr^{-1}) inputs to the ocean of any river, representing ~18% and 6% of the global fluxes respectively (Milliman & Farnsworth, 2011). Ten surface water samples spanning a salinity range of 0.32 to 35.84 were analyzed for Ba concentration and isotope composition (Fig. 1a). These samples were collected along a transect following the northward transport of the Amazon freshwater plume, from the Amazon mouth and along the continental shelf towards Barbados, in March, 1996 as described by Swarzenski et al. (2004). Samples were filtered (0.45 μm) prior to acidification by addition of distilled HCl.

The Fly River discharges into the Gulf of Papua, New Guinea with mean annual average freshwater and sediment discharge rates of 180 km^3 yr^{-1} and 110 Mt yr^{-1}, respectively (Milliman and Farnsworth, 2011). It has a very high sediment yield (1.5 Mt km^{-2} yr^{-1}) and high average suspended sediment concentrations of 611 mg L^{-1} (Milliman and Farnsworth, 2011). Six surface water samples spanning a salinity range of 2 to 35 were measured for Ba concentration and isotope composition (Fig. 1b). These samples

were collected across the estuarine mixing zone of the Fly River in September 1997, as described by Swarzenski et al. (2004). Samples were filtered (0.45 μm) prior to acidification by addition of distilled HCl.

The Johor River discharges into the Johor and Singapore Straits with average freshwater and sediment discharge rates of 2.4 km^3 yr^{-1} and 1.2 to 2.9 Mt yr^{-1} respectively (Milliman and Farnsworth, 2011, van Maren et al., 2014). Eight surface water samples spanning a salinity range of 0 to 27 along the Johor River estuary were measured for Ba concentration and isotopes composition (Fig. 1cd). Water samples were collected using trace-metal cleaned bottles, transported in dark, cool conditions back to the laboratory where they were filtered (0.45 μm Nuclepore polycarbonate filters) and acidified following trace metal clean procedures (Chen et al., 2015).

3. Analytical techniques

The Ba concentrations and isotope compositions of waters were determined using thermal ionization mass spectrometry (TIMS; TRITON instrument, Thermo Scientific), and a previously described double spike technique to correct for instrumental mass bias (Hsieh & Henderson, 2017). Sample aliquots of 50 ml (Amazon and Fly samples) and 2 to 30 ml (Johor samples) were accurately weighed and equilibrated with a known quantity of a ^{135}Ba-^{137}Ba double spike solution. Three of the spiked Johor samples (salinities 0, 8 and 9), and one of the Amazon samples (salinity 0.32) were evaporated to dryness and refluxed in 1 ml 15M HNO_3 to digest any organic material. The mass of total dissolved material in the remainder of the spiked sample aliquots required the pre-concentration of Ba by co-precipitation with $CaCO_3$ (Foster et al., 2004). To achieve this, samples with salinities <20 were first partially evaporated to increase their salinities to about 30, while

151 samples with salinities >20 were subject co-precipitation directly, induced by the addition
152 of 1 ml 0.9 M Na_2CO_3 solution per 16 ml of sample. The Na_2CO_3 solution was pre-
153 cleaned by inducing $CaCO_3$ precipitation as previously described (Hsieh and Henderson,
154 2017). The $CaCO_3$ precipitates were separated by centrifugation, and washed in 15 ml
155 MilliQ water. The dried sample residues and the $CaCO_3$ precipitates were dissolved in 1
156 ml 3M HCl and processed through a cation exchange procedure (Supplementary
157 Information). The eluted Ba fractions were dried and any organics that were leached from
158 the cation exchange resin were oxidized prior to TIMS analyses by addition and
159 evaporation of 15 M HNO_3 and 9.8 M H_2O_2. The procedural blanks were determined to
160 be 0.05 – 3.72 ng of Ba (n = 4, total range), representing <1.4% of the Ba processed in the
161 samples.
162 Barium isotope measurements using TIMS featured a double Re filament
163 assembly following previously described protocols (Hsieh & Henderson, 2017,
164 Bridgestock et al., 2019). Briefly, during each analysis, ion beams at atomic masses 134
165 (Ba), 135 (Ba), 136 (Ba), 137 (Ba), 138 (Ba), 139 (La) and 140 (Ce) were monitored
166 simultaneously using Faraday cups equipped with 10^{11} Ω resistors. Barium isotope
167 compositions are expressed as $\delta^{138/134}$Ba values (eqn. 1) relative to the standard reference
168 material NIST 3104a:
169
170 $$\delta^{138/134}\text{Ba ‰} = \left(\frac{^{138}\text{Ba}/^{134}\text{Ba}_{\text{sample}}}{^{138}\text{Ba}/^{134}\text{Ba}_{\text{NIST3104a}}} - 1\right) \times 1000 \quad (1)$$
171
172 Repeat measurements of NIST 3104a over a period of 12 months, run at ion beam
173 intensities of 6 to 10 V on ^{138}Ba, comparable to the majority of sample analyses, yielded a
174 reproducibility of ± 0.03 ‰ (2SD, n = 12). This is taken to represent the level of
175 uncertainty for Ba isotope analyses for the majority of samples. Analyses of one sample

from the Amazon plume (at salinity 34.58) featured lower ion beam intensities, with uncertainty is taken as the internal reproducibility (± 0.04 ‰ 2SE) of the individual analysis. To validate the accuracy of the isotope analyses, a secondary inter-laboratory $BaSO_4$ standard, NBS-127, was analyzed during every measurement session, and this yielded $\delta^{138/134}Ba$ = -0.29 ± 0.02 ‰ (mean ± 2SD, n = 14), in agreement with published values ($\delta^{138/134}Ba$ = -0.27 ± 0.02 ‰; Horner et al., 2017, and -0.29 ± 0.01 ‰; Crockford et al., 2019).

Barium concentrations were calculated from the isotopic analyses by isotope dilution. For the Amazon and Johor River estuary samples, Ba concentrations were also determined by inductively coupled plasma mass spectrometry and agree within 12 % of those determined by TIMS (Table 1) (Supplementary Information). Barium concentrations for the Fly River samples have been previously published (Swarzenski et al., 2004). These values agree within 8 to 31% of those determined in this study from the TIMS analyses, with the exception of the sample at salinity 4 for which the Ba concentration presented in this study is 54% higher. The reason for this disagreement is unknown. We consider the Ba concentrations obtained by isotope dilution from the TIMS analyses to be more accurate, so where available these results are presented and discussed in the following.

4. Results

The distribution of Ba concentrations in the Amazon freshwater plume as a function of salinity are in agreement with previously published results (Boyle, 1976) (Fig. 2, Table 1). The lowest salinity sample (0.32), which is taken to reflect that of Amazon River water, features a Ba concentration of 124 nmol kg^{-1} consistent with published

values (129 to 150 nmol kg^{-1}; Boyle, 1976, Gaillardet et al., 1997, Cao et al., 2020). Barium concentrations increase with salinity to a maximum of 243 nmol kg^{-1} at salinity 5.6, before decreasing linearly to 37 nmol kg^{-1} at salinity 35.84 (Boyle, 1976, this study). Amazon River water features a $\delta^{138/134}$Ba of 0.15 ‰, which agrees within analytical uncertainty with that determined by Cao et al. (2020), of 0.14 ± 0.02 ‰. At salinity 16.31, $\delta^{138/134}$Ba decreases to 0.04 ‰, before increasing to 0.54 ‰ at salinity 35.4, which is in agreement with published data for North Atlantic surface waters ($\delta^{138/134}$Ba = 0.46 to 0.57 ‰; Bates et al., 2017, Hsieh & Henderson, 2017, Hemsing et al., 2018). These samples between salinities 16.31 and 35.84 display a linear correlation between $\delta^{138/134}$Ba and 1/Ba concentrations ($r^2 = 0.96$; Fig. 2c).

In the Fly River estuary, Ba concentrations increase from 143 nmol kg^{-1} at salinity 0 to a maximum of 509 nmol kg^{-1} at salinity 4 (Fig. 3, Table 1; Swarzenski et al., 2004, this study). Between salinity 4 and 35, Ba concentrations display a negative linear correlation with salinity ($r^2 = 0.92$), decreasing to 63 nmol kg^{-1} at salinity 35. The sample at salinity 2 features a $\delta^{138/134}$Ba value of 0.19 ‰, decreasing to relatively constant $\delta^{138/134}$Ba values of about 0.1 ‰ between salinities 4 and 25, before increasing to 0.33 ‰ at salinity 35. Samples between salinity 4 and 25 display a linear correlation between $\delta^{138/134}$Ba and 1/Ba concentrations ($r^2 = 0.88$; Fig. 3c). No Ba isotope data are available for the river water (salinity 0) endmember of this estuary.

In the Johor River estuary, Ba concentrations increase from 352 nmol kg^{-1} at salinity 0, to 838 nmol kg^{-1} at salinity 8 (Fig.4, Table 1). Between salinities 8 and 27, Ba concentrations are negatively correlated with salinity ($r^2 = 0.91$), with the exception of the sample from a separate tributary, which lies below this relationship and is excluded from the regression. Likewise the $\delta^{138/134}$Ba values decrease from 0.19 ‰ at salinity 0 to -0.02 ‰ at the Ba concentration maximum (salinity 8), before systematically increasing to 0.34

226 ‰ at salinity 27. Samples between salinities 8 and 27 display a linear correlation between
227 $\delta^{138/134}$Ba and 1/Ba concentration ($r^2 = 0.75$; Fig. 4c).
228
229 **5. Discussion**
230
231 *5.1 Estuarine processes modify the $\delta^{138/134}$Ba of net riverine fluxes to the ocean*
232
233 The determined dissolved Ba concentration distributions in the Amazon, Fly and
234 Johor river estuaries (Fig. 2, 3 and 4) are typical of those observed in the majority of
235 previously studied estuaries (Boyle, 1976, Hanor and Chan, 1977, Edmond et al., 1978, Li
236 and Chan, 1979, Carroll et al., 1993, Swarzenski et al., 2004, Coffey et al., 1997, Guay
237 and Falkner, 1998, Stecher and Kogut, 1999, Nozaki et al., 2001, Joung and Shiller, 2014,
238 Samanta and Dalai, 2016, Hong et al., 2018). Dissolved Ba concentrations increase to
239 maximum values at mid salinities (~4 to 10) due to the addition of dissolved Ba by
240 estuarine processes. This is predominantly due to particulate Ba desorption (e.g. Hanor
241 and Chan, 1977), although in some estuaries benthic inputs may be important (Moore et
242 al, 1997, Colbert & McManus, 2005, Joung & Shiller, 2014, Hong et al., 2018). In higher
243 salinity regions of estuaries, linear relationships between dissolved Ba and salinity are
244 indicative of conservative mixing with seawater, as observed in the results presented here.
245 Notably, the higher salinity regions of the studied estuaries are also characterized by
246 linear relationships between $\delta^{138/134}$Ba and 1/Ba concentration, which are consistent with
247 conservative mixing with respect to $\delta^{138/134}$Ba. Extrapolation of these mixing relationships
248 to salinity 0 provides an estimate of 'effective' river endmember values (Fig. 2, 3 and 4)
249 (Supplementary Information), which is the theoretical Ba concentration or $\delta^{138/134}$Ba value
250 of a parcel of river water after modification by estuarine processes. The quantity and

isotope composition of Ba added to the dissolved flux due to estuarine processes can be estimated through comparison of the effective river Ba concentration and $\delta^{138/134}$Ba value to those measured for the riverine dissolved load (eqn. 2 and 3).

$$[Ba]_{added} = [Ba]_{effective} - [Ba]_{river} \quad \text{(eqn. 2)}$$

$$\delta^{138/134}Ba_{added} = 1/f_{added} \times [\delta^{138/134}Ba_{effective} - (\delta^{138/134}Ba_{river} \times f_{river})] \quad \text{(eqn. 3)}$$

With:

$$f_{added} = [Ba]_{added}/[Ba]_{effective} \quad \text{(eqn. 4)}$$

$$f_{river} = [Ba]_{river}/[Ba]_{effective} \quad \text{(eqn. 5)}$$

The subscripts 'effective', 'river' and 'added' refer to the Ba concentration ([Ba]) and $\delta^{138/134}$Ba values of the effective river endmember, riverine dissolved load and the Ba added by estuarine processes (per kg of river water) respectively. For the Fly River estuary, measurement of the $\delta^{138/134}$Ba of the riverine dissolved load is not available. Instead $\delta^{138/134}Ba_{added}$ and $\delta^{138/134}Ba_{river}$ are estimated using mass balance calculations based on the data for the sample at salinity 2 and the effective river endmember (Supplementary Information).

Extrapolation of the conservative mixing data for each river are used to calculate estimated effective river Ba concentrations and $\delta^{138/134}$Ba values, along with the estimated amount and $\delta^{138/134}$Ba value of dissolved Ba added by processes in the Amazon, Fly and Johor river estuaries (Table 2). These calculations reveal that estuarine processes lower the $\delta^{138/134}$Ba of net riverine fluxes to the ocean (i.e. effective river endmembers) by 0.13 to 0.23 ‰ compared to those of riverine dissolved loads (Fig. 2, 3 and 4), due to the

addition of Ba featuring $\delta^{138/134}$Ba between 0.20 to 0.32 ‰ lower than the corresponding dissolved loads.

Next the potential importance of desorption from suspended riverine particles versus benthic inputs for controlling the addition of isotopically light Ba to the dissolved phase in the Amazon, Fly and Johor river estuaries are assessed. The Amazon and Fly rivers, respectively, have average suspended sediment concentrations of 191 mg L^{-1} and 611 mg L^{-1} (Milliman and Farnsworth, 2011), with concentrations up to 1500 mg L^{-1} and 1000 mg L^{-1} measured in the 3 to 8 salinity zones of these estuaries at the time of sample collection (Swarzenski et al., 2004). At these suspended sediment concentrations, exchangeable particulate Ba concentrations of 0.1 to 0.8 nmol mg^{-1} and of 0.3 to 0.5 nmol mg^{-1} would be required to supply the amount of Ba added in the Amazon and Fly River estuaries, respectively (Table 2). These values are within the range of exchangeable Ba concentrations (0.12 and 1.7 nmol mg^{-1} of sediment) determined for suspended particles from other rivers (Yellow, Humber, Hooghly, and Hudson; Li and Chan, 1979, Coffey et al., 1997, Samanta and Dalai, 2016, Gou et al., 2020). Particulate Ba desorption can therefore feasibly account for the observed Ba addition in the Amazon and Fly River estuaries.

Suspended sediment concentrations in the Johor River are poorly constrained at ~150 mg L^{-1} (average), possibly ranging up to ~1000 mg L^{-1} during high discharge events (van Maren et al., 2014). These suspended sediment concentrations require exchangeable particulate Ba concentrations of 0.7 to 4.6 nmol mg^{-1} to account for the observed estuarine Ba addition, of 688 nmol kg^{-1}. This range overlaps but exceeds exchangeable Ba concentrations measured for riverine particles (0.12 to 1.7 nmol mg^{-1}; Li and Chan, 1979, Coffey et al., 1997, Samanta and Dalai, 2016, Gou et al., 2020). In this case, significant

benthic inputs cannot be ruled out, but are not necessarily required to explain the magnitude of dissolved Ba addition in the Johor River estuary.

5.2 Insights into the controls on the $\delta^{138/134}$Ba of river dissolved loads

Previous studies have noted that river dissolved loads are offset to higher $\delta^{138/134}$Ba values than the weathering lithologies (Gong et al., 2019, Gou et al., 2020, Charbonnier et al., 2020). Compiled $\delta^{138/134}$Ba data for the dissolved loads of 12 different rivers are systematically higher that the average $\delta^{138/134}$Ba of rocks further supporting this observation (Fig. 5) (Miyazaki et al., 2014, Nan et al., 2015, van Zuilen et al., 2016, Bullen and Chadwick, 2016, Bridgestock et al., 2018, Nielsen et al., 2018, Nan et al., 2018, Gou et al., 2020, Cao et al., 2020, Nielsen et al., 2020, An et al., 2020, Lin et al., 2020, Tieman et al., 2020, this study). The available $\delta^{138/134}$Ba for rocks display a significant total range of -0.63 to 0.37 ‰, however the majority of rocks analyzed so far feature $\delta^{138/134}$Ba ≈ 0 ‰ (Fig. 5), as exemplified by the recent estimate of average upper continental crust $\delta^{138/134}$Ba of 0.00 ± 0.04 ‰ (Nan et al., 2018). Lithological $\delta^{138/134}$Ba variability therefore cannot explain the systematic offset of river dissolved loads to higher $\delta^{138/134}$Ba values, and is unlikely to significantly control river dissolved load $\delta^{138/134}$Ba variability, particularly in larger river catchments where integration towards the average $\delta^{138/134}$Ba of rocks might be expected. The systematic offset of riverine dissolved loads to higher $\delta^{138/134}$Ba relative to average rock values therefore requires Ba isotope fractionation during processes operating within the critical zone.

Recent studies have argued that preferential adsorption of lighter Ba isotopes within soils and suspended riverine sediments can explain the offset between the $\delta^{138/134}$Ba of river dissolved loads and those of the weathering lithologies (Gong et al.,

2019, 2020, Gou et al., 2020). The magnitude of this isotope fractionation however remains poorly constrained. Isotope fractionations accompanying additional processes such as the leaching of Ba from primary minerals (Gong et al., 2020), Ba uptake into biomass (Bullen and Chadwick, 2016) and secondary mineral precipitation (Gou et al., 2020) may also influence river dissolved load $\delta^{138/134}$Ba. In particular, $\delta^{138/134}$Ba data for river waters from the Amazon River basin were recently interpreted as being controlled by a combination of isotope fractionations during Ba incorporation into secondary minerals, and uptake into terrestrial biomass (Charbonnier et al., 2020).

Our results indicate that Ba desorbed from riverine suspended particles within estuaries features lower $\delta^{138/134}$Ba than corresponding river dissolved loads (Fig. 2, 3 and 4, Table 2). Desorption of exchangeable particulate Ba from suspended sediment in response to changes in salinity in estuaries is thought to be quantitative (Li et al., 1984, Samanta & Dalai, 2016). The isotope composition calculated for the addition flux ($\delta^{138/134}$Ba = -0.11 ± 0.13 ‰, +0.02 ± 0.15 ‰ and -0.01 ± 0.19 ‰ for the Amazon, Fly, Johor Rivers respectively; Table 2) is therefore likely to represent that of exchangeable Ba transported on riverine particles. The offset between these compositions and those of the corresponding river dissolved loads likely reflect isotope fractionations during the adsorption of Ba onto particle surfaces, of $\Delta^{138/134}Ba_{dissolved\text{-}adsorbed}$ = -0.26 ± 0.14 ‰, -0.32 ± 0.28 ‰ and -0.20 ± 0.19 ‰ for the Amazon, Fly and Johor rivers respectively (where $\Delta^{138/134}Ba_{dissolved\text{-}adsorbed} = \delta^{138/134}Ba_{river} - \delta^{138/134}Ba_{added}$; Table 2). It is interesting to note the consistency of these estimated isotope fractionation factors between these three river systems, although the propagated uncertainties on these values are large. In detail, the magnitudes of isotope fractionations accompanying Ba adsorption in river catchments are likely to depend on numerous factors, including the composition of suspended particulate loads as well as river water pH, ionic strength and major ion compositions, requiring

350 further study through direct measurements of exchangeable particulate Ba isotope
351 compositions.
352 In contrast to riverine dissolved loads, the effective river $\delta^{138/134}$Ba values for the
353 Amazon, Fly and Johor are comparable to the upper continental crust/average rock
354 $\delta^{138/134}$Ba (Fig. 6). Hsieh and Henderson (2017) also report an effective river $\delta^{138/134}$Ba of
355 0.03 ± 0.09 ‰ for the combined discharge of the Paraná and Uruguay rivers from the Rio
356 de la Plata estuary (670 km^3 yr^{-1}; Milliman and Farnsworth, 2011) also in agreement with
357 the upper continental crust. In other words the combined dissolved and adsorbed Ba pools
358 transported in these rivers are in isotopic balance with the expected average composition
359 weathering lithologies in these catchments (Fig. 6). This supports the idea that isotopic
360 fractionation accompanying Ba adsorption onto particle surfaces is an important control
361 on riverine dissolved load $\delta^{138/134}$Ba variations (Gong et al., 2019, 2020, Gou et al., 2020).
362 It implies that additional processes such as Ba uptake into biomass and secondary
363 minerals, or incongruent weathering of primary minerals do not significantly influence
364 dissolved load $\delta^{138/134}$Ba of the studied rivers, or that effects of such processes happen to
365 cancel each other out.
366 A recent study discounted Ba adsorption as an important process for explaining
367 the systematic offset of river dissolved loads in the Amazon River basin to higher
368 $\delta^{138/134}$Ba weathering lithology, instead favoring isotope fractionations accompanying Ba
369 uptake into secondary minerals and terrestrial organic matter as the dominant control
370 (Charbonnier et al., 2021). Our results for the Amazon River estuary however suggest that
371 Ba adsorption to suspended sediments can explain this offset, at least at the mouth of this
372 river, at the time of sampling. Coupled measurements of dissolved and adsorbed Ba pools
373 transported by rivers will be required to further unravel the processes responsible for

374 controlling river dissolved load $\delta^{138/134}$Ba, and hence the development of this novel
375 isotope system trace critical zone processes.
376
377 *5.3 Towards balancing the marine barium isotope budget*
378
379 *5.3.1 Estimating the global riverine Ba flux to the ocean*
380
381 Rivers have previously been considered to be the dominant source of Ba to the
382 ocean, with additional inputs from submarine groundwater discharge and hydrothermal
383 vents (Wolgemuth and Broecker, 1970, Paytan and Kastner, 1996, Shaw et al., 1998,
384 Dickens et al., 2003). Wolgemuth and Broecker (1970) and Gaillardet et al. (2003)
385 estimate global riverine dissolved Ba fluxes of 10.5 Gmol yr^{-1} and 6.3 Gmol yr^{-1}
386 respectively. These flux estimates however, are based on only riverine dissolved load data
387 and do not account for the release of dissolved Ba within estuaries. Using the effective
388 river Ba concentration reported for the Congo River (Edmond et al., 1978), Paytan and
389 Kastner (1996) estimated a global riverine dissolved Ba flux to the ocean of 10.6 Gmol yr^{-1}
390 . This latter estimate accounts for estuarine release of dissolved Ba, but relies upon a
391 single value for the Congo River to be globally representative.
392 To improve on previous global riverine Ba flux estimates, literature data for 47
393 estuarine dissolved Ba concentration distributions from 27 different rivers have been
394 compiled (Table 3, Supplementary Information, Electronic Data). From each of these
395 estuarine dissolved Ba concentration distributions we calculated the Ba concentration of
396 the river dissolved load ($[Ba]_{river}$) and the effective river ($[Ba]_{effective}$) endmembers as
397 described in section 5.1 and the Supplementary Information file. A detailed description

398 and analysis of this compiled dataset is given in the Supplement Information file, and is
399 summarized in the following.
400 The majority of the estuarine Ba distributions (35 out of the 38 distributions for
401 which there are constraints on $[Ba]_{river}$) yield $[Ba]_{effective}$ that are significantly higher than
402 $[Ba]_{river}$. This highlights the global importance of estuarine processes for increasing net
403 riverine Ba fluxes to the ocean. Desorption of Ba from suspended particles is interpreted
404 to be the dominant process for driving this estuarine Ba addition (e.g. Hanor and Chan,
405 1977, Edmond et al., 1987, Li and Chan, 1979), however, inputs from submarine
406 groundwater discharge or diagenetic release from estuarine bottom sediments have also
407 been invoked to explain some of these estuarine Ba distributions (Frolich et al., 1985,
408 Moore, 1997, Moore and Shaw, 2008, Joung and Shiller, 2014, Hong et al., 2018). The
409 magnitude of estuarine Ba addition (calculated following eqn. 2) for the rivers in the
410 compilation increases with suspended sediment concentration (Fig. 7). Furthermore, the
411 magnitude of estuarine Ba addition for the majority of the rivers can be explained by
412 levels of Ba release per mass of sediment that are in range of measured riverine suspended
413 sediment exchangeable Ba concentrations (0.12 to 1.7 nmol mg^{-1}; Li and Chan, 1979,
414 Coffey et al., 1997, Samanta and Dalai, 2016, Gou et al., 2020) (Fig. 7). This further
415 supports the global importance Ba desorption from suspended river sediments in
416 estuaries, and highlights sediment discharge as a key control on net riverine Ba fluxes to
417 the ocean.
418 The combined discharge of the 27 rivers in the literature compilation is 13400 km^3
419 yr^{-1}, representing 37% of the global freshwater flux to the ocean of 36000 km^3 yr^{-1} (Table
420 3) (Milliman and Farnsworth, 2011). The discharge weighed average $[Ba]_{river}$ and
421 $[Ba]_{effective}$ of the 27 rivers in the literature compilation are 155 and 282 nmol kg^{-1}
422 respectively. Combined with a global riverine freshwater flux to the ocean of 36000 km^3

423 yr^{-1} (Milliman and Farnsworth, 2011), yields a global net riverine Ba input to the ocean of
424 10.1 Gmol yr^{-1} (based on $[Ba]_{effective}$), of which 5.6 Gmol yr^{-1} is transported by river
425 dissolved loads (based on $[Ba]_{river}$). There are two major sources of uncertainty on these
426 estimates. Firstly, due to temporal variations in $[Ba]_{river}$ and $[Ba]_{effective}$ for individual
427 rivers, which are likely on the order of ± 50% based on the rivers for which multiple
428 estuarine Ba distributions spanning different time periods are available in the compiled
429 dataset (Supplementary Information). Secondly there is uncertainty in how well these
430 discharge weighted average $[Ba]_{river}$ and $[Ba]_{effective}$ represent the 63% of the global
431 riverine freshwater flux discharged by rivers not included in the compiled literature data.
432 In particular, the discharge weighted average $[Ba]_{river}$ and $[Ba]_{effective}$ are strongly biased
433 towards those of the Amazon River, which accounts for 50% of the total discharge of the
434 rivers in the compilation. Using the un-weighed average $[Ba]_{river}$ and $[Ba]_{effective}$ of the
435 rivers in the data compilation of 296 and 387 nmol kg^{-1} respectively, may therefore better
436 represent globally averaged values. These values yield a global net riverine Ba input to
437 the ocean of 13.9 Gmol yr^{-1} (based on $[Ba]_{effective}$) of which 10.7 Gmol yr^{-1} transported by
438 river dissolved loads (based on $[Ba]_{river}$).
439 A further bias, impacting the both of the flux estimates above, is that the average
440 suspended sediment concentration of the rivers in the data compilation (of 253 mg L^{-1}) is
441 about half the global average (528 mg L^{-1}; Milliman and Farnsworth, 2011). This bias
442 reflects the importance of small (< 10000 km^2), mountainous rivers catchments for
443 supplying up to 45% of the global sediment flux (Milliman and Farnsworth, 2011), which
444 are poorly represented in the compilation. Given the role of sediment discharge for
445 driving estuarine Ba release via desorption from suspended sediments (Fig. 7), global
446 riverine Ba flux estimates based on the compiled data therefore likely underestimate the
447 true value. The compiled literature data suggest typical estuarine desorption of between

448 0.3 and 0.7 nmol of Ba per mg of suspended river sediment (Fig. 7). Coupling these
449 values with a global average riverine suspended sediment concentration of 528 mg L^{-1},
450 and global riverine freshwater discharge of 36000 km^3 yr^{-1} (Milliman and Farnsworth,
451 2011), yields a global estuarine Ba release of 5.7 to 13.3 Gmol yr^{-1}. Combined with the
452 estimates of river dissolved load global Ba fluxes above (5.6 and 10.7 Gmol yr^{-1}) yields
453 estimates of global net riverine Ba fluxes to the ocean of between 11.3 and 24 Gmol yr^{-1}.
454 Based on the above discussion we suggest that the global net riverine Ba flux to
455 the ocean is likely ~10 to 20 Gmol yr^{-1}, with between ~20 to 75 % of this flux derived
456 from estuarine processes. These estimates remain subject to large uncertainty, but
457 represent a significant advancement on previous estimates. Improving on these flux
458 estimates requires more data for estuarine Ba distributions, particularly for rivers with
459 large suspended sediment loads, which likely play an important role in supplying Ba to
460 the ocean via desorption from suspended riverine sediment (Fig. 7).
461
462 *5.3.2. The importance of riverine marine Ba inputs compared to other marine Ba sources*
463
464 In comparison to our global net riverine dissolved Ba flux estimate of ~10 to 20
465 Gmol yr^{-1}, the global dissolved Ba flux by submarine groundwater discharge (SGD) has
466 recently been estimated to be between 0.4 and 3.6 Gmol yr^{-1} (Mayfield et al., 2021). This
467 estimate however only accounts for the freshwater component of the global marine Ba
468 input from SGD. Re-circulation of seawater through coastal sediments represents another
469 important component of SGD chemical fluxes to the ocean (Swarzenski, 2007), which has
470 been shown to provide Ba inputs that exceed riverine Ba inputs in certain coastal regions
471 (Shaw et al., 1998, Moore and Shaw, 2008). The global importance of this saline
472 component of the SGD Ba input to the ocean however remains unconstrained. The Ba in

this saline component of SGD is derived from diagenetic reactions in coastal sediment, rather than from terrestrial chemical weathering. It is therefore unclear as to how much of this source truly represents an input of 'new' Ba to the ocean, rather than the recycling of Ba recently removed from seawater.

Dissolved Ba inputs from hydrothermal vents have previously been estimated at 2.40 to 3.35 Gmol yr^{-1} (Paytan and Kastner, 1996, Dickens et al., 2003), based on the extremely high Ba concentrations of hydrothermal fluids (>10 μmol kg^{-1}; Von Damm et al., 1985). The vast majority of this Ba is however known to precipitate as $BaSO_4$ during mixing of hydrothermal fluids with deep ocean waters (e.g. Jamieson et al., 2016), significantly reducing the magnitude of this input. There is considerable uncertainty regarding the extent to which this process reduces the hydrothermal Ba input, but it is likely that 'effective' Ba concentration of these hydrothermal inputs are close to deep ocean concentrations (<200 nmol kg^{-1}; Hsieh et al., 2021). Coupled with a hydrothermal water flux of 3×10^{13} kg yr^{-1} (Elderfield and Schultz, 1996) results in hydrothermal Ba fluxes several orders of magnitude lower than previous estimates (<0.006 Gmol yr^{-1}), which are negligible compared to the estimated global net riverine Ba flux (~10 to 20 Gmol yr^{-1}).

In summary, the flux estimates discussed above support previous assertions that rivers are the dominant input of Ba to the ocean. We however caution that all of these flux estimates have a high degree of uncertainty, and that the importance of Ba inputs from the recirculated seawater component of SGD (e.g. Moore and Shaw, 2008) needs to be further developed as it could be an important component of the marine Ba budget.

5.3.3. Constraints on the marine Ba isotope budget

The main output of Ba from the ocean is though the precipitation of $BaSO_4$ and its burial in marine sediment (e.g. Paytan and Kastner, 1996, Dickens et al., 2003). The currently available $\delta^{138/134}$Ba data for riverine dissolved loads are systematically higher than $BaSO_4$ in modern ocean sediment of 0.04 ± 0.06 ‰ (mean ± 2sd, n = 61; Crockford et al., 2019) (Fig. 5, 6). Furthermore, recent constraints on the $\delta^{138/134}$Ba of the freshwater component of submarine groundwater discharge and hydrothermal inputs, of 0.12 ± 0.03 ‰ and 1.7 ± 0.07 ‰, respectively are also systematically higher that this output (Hsieh et al., 2021, Mayfield et al., 2021). This suggests that either the marine Ba isotope budget is currently not in steady state, or that there are important additional sources featuring low $\delta^{138/134}$Ba or sinks featuring high $\delta^{138/134}$Ba missing from this budget. In this regard, the findings presented in this study, that estuarine processes lower the $\delta^{138/134}$Ba of net river inputs to the ocean represents an important step towards balancing the marine Ba isotope budget. Specifically the Ba flux weighted (0.02 ± 0.05 ‰) and un-weighted (0.05 ± 0.05 ‰) means (±2sd) of the effective river $\delta^{138/134}$Ba for the Amazon, Rio de la Plata, Fly and Johor river systems agree with the mean $\delta^{138/134}$Ba of marine $BaSO_4$ (Fig. 6). These rivers represent ~20 % of the global freshwater discharge and ~9 to ~19 % of our estimate for the global net dissolved riverine Ba flux to the ocean (Table 3). It remains unclear as to how representative these four values are of the $\delta^{138/134}$Ba of global net dissolved riverine fluxes to the ocean, given the potential for both temporal variability within the studied river systems and variability between river systems. Nevertheless, it is clear that accounting for the release of low $\delta^{138/134}$Ba due to desorption from riverine suspended particles in estuaries, as documented by this study, is important to constrain the modern marine Ba isotope budget. Thus, river dissolved load $\delta^{138/134}$Ba data do not necessarily represent the isotope composition of the riverine Ba inputs to the ocean, and more data

522 spanning estuarine mixing zones is required to properly assess the $\delta^{138/134}$Ba of global net
523 riverine Ba inputs to the ocean.
524
525 **6. Conclusions**
526
527 The isotope compositions of net dissolved riverine Ba fluxes to the ocean are
528 foremost modified by particulate Ba desorption in estuaries. This process contributes Ba
529 featuring $\delta^{138/134}$Ba that is about 0.2 to 0.3 ‰ lower than corresponding river dissolved
530 loads, an offset that likely reflects an isotope fractionation during the adsorption of Ba
531 released during chemical weathering onto mineral surfaces. This supports the idea that
532 preferential adsorption of lighter Ba isotopes is a key process for controlling $\delta^{138/134}$Ba
533 values of riverine dissolved loads, as previously suggested (Gong et al., 2019, 2020, Gou
534 et al., 2020).
535 Net dissolved riverine Ba fluxes to the ocean are a globally important marine Ba
536 source, which we estimate to be ~10 to 20 Gmol yr^{-1}, a significant component of which is
537 derived from particulate Ba desorption in estuaries. River dissolved loads are
538 systematically offset to higher $\delta^{138/134}$Ba than the main output of dissolved Ba from the
539 ocean, burial of marine $BaSO_4$, contributing to an apparent imbalance in the marine Ba
540 isotope budget. Our results demonstrate that accounting for estuarine processes is
541 necessary to properly assess the $\delta^{138/134}$Ba of net riverine Ba fluxes to the ocean, and in
542 doing so will likely play a key role towards balancing the modern marine Ba isotope
543 budget.
544
545 **Acknowledgements**
546

Luke Bridgestock was supported by a Leverhulme Trust Early Career Fellowship (ECF-2019-049) for part of this research. The collection of Johor River estuary samples was supported by funding from the Singapore National Research Foundation (NRF), Prime Minister's Office, under the Marine Science Research and Development Programme (Project MSRDP-03) and the Royal Society's Commonwealth Science Grant (CSC\R1\170048). The IAEA is grateful for the support provided to its Environment Laboratories by the Government of the Principality of Monaco. We thank two anonymous reviewers and the handling editor, Christian France-Lanord, for their feedback, which helped to greatly improve this manuscript.

References

An, Y-J., Li, X. and Zhang, Z-F. (2020) Barium isotopic compositions in thirty-four geological reference materials analysed by MC-ICP-MS, *Geostandards and Geoanalytical Research*, **44**, 183-199, doi:10.1111/ggr.12299

Bates S. L., Hendry K. R., Pryer H. V., Kinsley C. K., Pyle K. M., Woodward E. M. and Horner T. J. (2017) Barium isotopes reveal role of ocean circulation on barium cycling in the Atlantic*, Geochimica and Cosmochimica Acta,* **204**, 286-299, doi: 10.1016/j.gca.2017.01.043

Boyle E. A. (1976) The marine geochemistry of trace metals, PhD Thesis, Massachusetts Institute of Technology

Bridgestock L., Hsieh Y-T., Porcelli D., Homoky W. B., Bryan A. and Henderson G. M. (2018) Controls on the barium isotope compositions of marine sediments, *Earth and Planetary Science Letters*, **481**, 101-110, doi: 10.1016/j.epsl.2017.10.019

Bridgestock L., Hsieh Y-T., Porcelli D. and Henderson G. M. (2019) Increased export production during recovery from the Paleocene-Eocene thermal maximum constrained by sedimentary Ba isotopes, *Earth and Planetary Science Letters,* **510**, 53-63, doi:10.1016/j.epsl.2018.12.036

Bullen T. and Chadwick O. (2016) Ca, Sr and Ba stable isotopes reveal the fate of soil nutrients along a tropical climosequence in Hawaii, *Chemical Geology*, **422**, 25-45, doi:10.1016/j.chemgeo.2015.12.008

Cao, Z., Siebert, C., Hathorne, E. C., Dai, M. and Frank, M. (2020) Corrigendum to "Constraining the oceanic barium cycle with stable barium isotopes", *Earth and Planetary Science Letters*, **530**, 116003, doi:10.1016/j.epsl.2015.11.017

Carroll J., Falkner K. K. Brown E. T. and Moore W. S. (1993) The role of the Ganges-Brahmaputra mixing zone in supplying barium and ^{226}Ra to the Bay of Bengal, *Geochimica and Cosmochimica Acta*, **57**, 2981-2990

Charbonnier Q., Bouchez J., Gaillardet J. and Gayer E. (2020) Barium stable isotopes as a fingerprint of biological cycling in the Amazon River basin, *Biogeosciences*, **17**, 5989-6015, doi:10.5194/bg-17-5989-2020

Chen M. L., Lee J-M., Nurhati I. S., Switzer A. D. and Boyle E. A. (2015) Isotopic record of lead in Singapore Straits during the last 50 years: spatial and temporal variations, *Marine Chemistry*, **168**, 49–59.

Coffey M, Dehairs F., Collette O., Luther G., Church T. and Jickells T. (1997) The behaviour of dissolved barium in estuaries, *Coastal and Shelf Science*, **45**, 113-121

Colbert D. and McManus J. (2005) Importance of seasonal variability and coastal processes on estuarine manganese and barium cycling in a Pacific Northwest estuary, *Continental Shelf Research*, **25**, 1395-1414, doi:10.1016/j.csr.2005.02.003

Crockford P. W., Wing B. A., Paytan A., Hodgskiss M. S. W., Mayfield K. K., Hayles J. A., Middleton J. E., Ahn A-S. C., Johnson D. T., Caxito F., Uhlein G., Halverson, G. P., Eickmann B., Torres M. and Horner T. J. (2019) Barium-isotopic constraints on the origin of post-Marinoan barites, *Earth and Planetary Science*, **519**, 234-244, doi:10.1016/j.epsl.2019.05.018

Dickens G. R., Fewless T., Thomas E. and Bralower T. J. (2003) Excess barite accumulation during the Paleocene-Eocene Thermal Maximum: Massive input of dissolved barium from seafloor gas hydrate reservoirs. *In Causes and consequences of globally warm climates in the early Paleogene* (eds Ginerich P. et al.). Geological Society of America Special Paper **369**, 11-23

Edmond J. M., Boyle E. A., Drummond D., Grant B. and Mislick T., (1978) Desorption of barium in the plume of the Zaire (Congo) River, *Netherlands Journal of Sea Research*, **12**, 324-328

Edmond J. M., Spivack A., Grant B. C., Ming-Hui,H. Zexiam C., Sung C. and Xiushau Z. (1985) Chemical dynamics of the Changjiang estuary, *Continental Shelf Research*, **4**, 17-36

Elderfield H. and Schultz A. (1996) Mid-ocean ridge hydrothermal fluxes and the chemical composition of the ocean, *Annual Reviews of Earth and Planetary Sciences*, **24**, 191-224

Fleitmann D., Dunbar R. B., McCulloch M., Mudelsee M., Vuille M., McClanahan T. R., Cole J. E. and Eggins S. (2007) East African soil erosion recorded in a 300 year old coral colony from Kenya, *Geophysical Research Letters*, **34**, doi:10/1029/2006GL028525

635 Foster, D. A., Staubwasser, M. & Henderson, G. M. (2004) ^{226}Ra and Ba concentrations
636 in the Ross Sea measured with multicollector ICP mass spectrometry, *Marine*
637 *Chemistry*, **87**, 59-71, doi:10.1016/j.marchem.2004.02.003
638
639 Frolich P. N., Kaul L. W., Byrd J. T., Andreae M. O. and Roe K. K. (1985) Arsenic,
640 barium, germanium, tin, dimethylsufide and nutrient biogeochemistry in Charlotte
641 Harbor, Florida, a phosphorus-enriched estuary, *Estuarine, Coastal and Shelf*
642 *Science*, **20**, 239-264
643
644 Gaillardet J., Dupré B., Allègre C. and Négrel P. (1997) Chemical and physical
645 denudation in the Amazon River Basin, *Chemical Geology*, **142**, 141-173
646
647 Gaillardet J., Viers J. and Dupré B. (2003), Trace elements in river waters, *In Treatise on*
648 *Geochemistry, Volume 5*, (eds. Drever J. I), doi:10.1016/B0-08-043751-6/05165-3
649
650 Gebregiorgis D., Hathorne E. C., Sijinkumar A. V., Nagender Nath B., Nürnberg, D. and
651 Frank M. (2016) South Asian summer monsoon variability during the last ~54 kyrs
652 inferred from surface water salinity and river runoff proxies, *Quaternary Science*
653 *Reviews*, **138**, 6-15, doi:10.1016/j.quascirev.2016.02.012
654
655 Geymann B. M., Ptacek J. L., LaVigne M. and Horner T. J. (2019) Barium in deep-sea
656 bamboo corals: Phase assocations, barium isotopes, and prospects for
657 paleoceanography, *Earth and Planetary Science Letters*, **525**, 115751,
658 doi:10.1016/j.epsl.2019.115751
659
660 Gong Y., Zheg Z., Zhou C., Nan X., Yu H., Lu Y., Li W., Gou W., Cheg W. and Huang
661 F. (2019) Barium isotope fractionation in latosol developed from strongly
662 weathered basalt, *Science of the Total Environment*, **687**, 1295-1304,
663 doi:10.1016/j.sdtotenv.2019.05.427
664
665 Gong, Y., Zeng, Z., Cheng, W., Lu, Y., Zhang, L., Yu, H. and Huang, F., (2020), Barium
666 isotopic fractionation during strong weathering of basalt in a tropical climate,
667 *Environment International*, **143,** 105896, doi:10.1016/j.envint.2020.105896
668
669 Gou L. and Deng L. (2019) Determination of barium isotopic ratios in river waters on
670 MC-ICP-MS, *Analytical Sciences*, doi:10.2116/analsci.18P329
671
672 Gou L., Jon Z., Galy A., Gong Y., Nan C. J., Wang X., Bouchez J., Cai H., Chen J., Yu
673 H. and Huang F. (2020) Seasonal riverine barium isotopic variation in the middle
674 Yellow River: Sources and Fractionation, *Earth and Planetary Science Letters*, **531**,
675 doi:10.1016/j.epsl.2019.115990
676
677 Guay C. K. and Falkner K. K. (1998) A survey of dissolved barium in the estuaries of
678 major Arctic rivers and adjacent seas, *Continental Shelf Research*, **18**, 859-882
679
680 Hanor J. S. and Chan L-H. (1977) Non-conservative behavior of barium during mixing of
681 Mississippi River and Gulf of Mexico waters, *Earth and Planetary Science Letters,*
682 **37**, 242-250
683

Hemsing F., Hsieh Y-T., Bridgestock L., Spooner P. T., Robinson L., F., Frank N. and Henderson G. M. (2018) Barium isotopes in cold-water corals, *Earth and Planetary Science Letters*, **491**, 183-192, doi: 10.1016/j.epsl.2018.03.040

Hong Q., Cai P., Geibert W., Cao Z., Stimac I., Liu L. and Li Q. (2018) Benthic fluxes of metals into the Pearl River Estuary based on 224Ra/228Th disequilibrium: From alkaline earth (Ba) to redox sensitive elements (U, Mn, Fe), *Geochimica and Cosmochimica Acta*, **237**, 223-239, doi:10.1016/j.gca.2018.06.036

Horner T. J. and Crockford P. W. (2021), Barium Isotopes: Drivers, Dependencies, and Distributions through Space and Time, *Elements in Geochemical Tracers in Earth System Science*, Cambridge: Cambridge University Press, doi:10.1017/9781108865845

Horner T. J., Kinsley C. W. and Nielsen S. G (2015) Barium isotope fractionation in seawater mediated by barite cycling and oceanic circulation, *Earth and Planetary Science Letters,* **430**, 511-522, doi:10.1016/j.epsl,2015.07.027

Horner T. J., Pryer H. V., Nielsen S. G., Crockford P. W., Gauglitz J. M., Wing B. A. and Ricketts R. D. (2017) Pelagic barite precipitation at micromolar ambient sulfate, *Nature Communications*, **8**, 1242, doi:10.1038/s41467-017-01229-5

Hsieh Y-T. and Henderson G. M. (2017) Barium stable isotopes in the global ocean: Tracer of Ba inputs and utilization, *Earth and Planetary Science Letters*, **473**, 269-278, doi:10.1016/j.epsl.2017.06.024

Hsieh Y-T., Bridgestock L., Scheuermann, P. P., Seyfried, W. E. and Henderson, G. M., (2021), Barium isotopes in mid-ocean ridge hydrothermal vent fluids: a source of isotopically heavy Ba to the ocean, *Geochimica and Cosmochimica Acta*, **292**, 348-363, doi:10.1016/j.gca.2020.09.037

Jamieson W. D., Hannington M. D., Tivey M. K., Hansteen T., Williamson N. M. B., Steward M., Fietzke J., Butterfield D., Frische M., Allen L., Cousens B. and Langer J. (2016) Precipitation and growth of barite within hydrothermal vent deposits from the Endeavour Segment, Juan de Fuca Ridge, *Geochimica and Cosmochimica Acta*, **173**, 64-85, doi:10.1016/j.gca.2015.10.021

Joung D., and Shiller A. M. (2014) Dissolved barium behavior in Louisiana Shelf waters affected by the Mississippi/Atchafalaya River mixing zone, *Geochimica and Cosmochimica Acta*, **141**, 303-313, doi:10/1016/j.gca.2014.06.021

Kipp L. E., Henderson P. B., Wang Z. A. and Charette M. A. (2020), Deltaic and estuarine controls on Mackenzie River solute fluxes to the Arctic Ocean, *Estuaries and Coasts*, doi:10.1007/s12237-020-00739-8

Lewis S. E., Lough J. M., Cantin N. E., Matson E. G., Kinsley L., Bainbridge Z. T. and Brodie J. E. (2018) A critical evaluation of coral Ba/Ca, Mn/Ca and Y/Ca ratios as indicators of terrestrial input: New data from the Great Barrier Reef, Australia, *Geochimica and Cosmochimica Acta,* **237**, 131-154, doi:10.1016/j.gca.2018.06.017

Li Y-H. and Chan L-H. (1979) Desorption of Ba and ^{226}Ra from river-borne sediments in the Hudson estuary, *Earth and Planetary Science Letters*, **43**, 343-350

Li Y-H., Burkhardt L. and Teraoka H. (1984) Desorption and coagulation of trace elements during estuarine mixing, *Geochimica and Cosmochimica Acta*, **48**, 1879-1884

Lin, Y-B., Wei, H-Z., Jiang, S-Y., Hohl, S., Lei, H-L., Liu, X. and Dong, G. (2020) Accurate determination of barium isotopic compositions in sequentially leached phases from carbonates by double spike-thermal ionization mass-spectrometry (DS-TIMS), *Analytical Chemistry*, **92**, 2417-2424, doi:10.1021/acs.analchem.9b03137

Mayfield, K. K., Eisenhauer, A., Santiago Ramos, D. P., Higgins, J. A., Horner, T. J., Auro, M., Magna, T., Moosdorf, N., Charette M. A., Gonneea, M. E., Brady, C. E., Komar, N., Peucker-Ehrenbrink, B. and Paytan, A. (2021) Groundwater discharge impacts marine isotope budgets of Li, Mg, Ca, Sr, and Ba, *Nature Communications*, doi:10.1038/s41467-020-20248-3

McCulloch M., Fallon S., Wyndham T., Hendy E., Lough J. and Barnes D. (2003) Coral record of increased sediment flux to the inner Great Barrier Reef since European settlement, *Nature,* **421**, 727-730, doi:10.1038/nature01361

Milliman J. D., and Farnsworth K. L. (2011) River discharge to the coastal ocean: a global synthesis, Cambridge University Press

Miyazaki T., Kimura J-I. and Chang Q. (2014) Analysis of stable isotope ratios of Ba by double spike standard-sample bracketing using multiple-collector inductively coupled plasma mass spectrometry, *J. Anal. At. Spectrom.,* **29**, 483-490, doi:10.1039/c3ja50311a

Moore W. S. (1997) High fluxes of radium and barium from the mouth of the Ganges-Brahmaputra River during low river discharge suggest a large groundwater source, *Earth and Planetary Science Letters*, **150**, 141-150

Moore W. S., and Shaw T. J. (2008) Fluxes and behavior of radium isotopes, barium, and uranium in seven Southeastern US rivers and estuaries, *Marine Chemistry*, **108**, 236-254, doi:10.1016/j.marchem,2007.03.004

Nan. X., Wu, F., Zhang, Z., Hou, Z., Haung, F. and Yu, H., (2015) High-precision barium isotope measurements by MC-ICP-MS, *J. Anal. At. Spectrom.,* doi:10.1039/c5ja00166h

Nan X-Y, Yu H-M., Rudnick R. L., Gaschnig R. M., Xu J., Li W-Y., Zhang Q., Jin Z-D, Li X-H. and Huang F. (2018) Barium isotopic composition of the upper continental crust, *Geochimica and Cosmochimica Acta*, **233**, 33-49, doi:10.1016/j.gca.2018.05.004

Nesbitt H. W., Markovics G. and Price R. C. (1980) Chemical processes affecting alkalis and alkaline earths during continental weathering, *Geochimica and Cosmochimica Acta*, **44**, 1659-1666

Nielsen S. G., Horner T. J., Pryer H. V., Blusztajn J., Shu, Y., Kurz, M. D., Le Roux V. (2018), Barium isotope evidence for pervasive sediment recycling in the upper mantle, *Science Advances,* **4**, eaas8675

Nielsen S. G., Shu Y., Auro M., Yogodzinski G., Shinjo R., Plank T., Kay S. M. and Horner T. J. (2020), Barium isotope systematics of subduction zones, *Geochimica and Cosmochimica Acta,* **275**, 1-18, doi:10.1016/j.gca.2020.02.006

Nozaki Y., Yamamoto Y., Manaka T., Amakawa H. and Snidvongs A. (2001) Dissolved barium and radium isotopes in the Chao Phraya River estuarine mixing zone in Thailand, *Continental Shelf Research,* **21**, 1435-1448

Paytan A. and Griffiths E. M. (2007) Marine barite: Recorder of variations in ocean export productivity, *Deep-Sea Research II*, **54**, 687-705, doi:10.1016/j.dsr.2007.01.007

Paytan A. and Kastner M. (1996) Benthic Ba fluxes in the central Equatorial Pacific, implications for the oceanic Ba cycle, *Earth and Planetary Science Letters*, **142**, 439-450

Price R. C., Gray C. M., Wilson R. E., Frey F. A. and Taylor S. R. (1991) The effects of weathering on rare-earth element, Y and Ba abundances in Tertiary basalts from southeastern Australia, *Chemical Geology*, **93**, 245-265

Samanta S. and Dalai T. K. (2016) Dissolved and particulate barium in the Ganga (Hooghly) River estuary, India: Solute-particle interactions and the enhanced dissolved flux to the oceans, *Geochimica and Cosmochimica Acta*, **195**, 1-28, doi:10.1016/j.gca.2016.09.005

Shaw T. J., Moore W. S., Kloepfer J. and Sochaski M. A. (1998) The flux of barium to the coastal waters of the southeastern USA: The importance of submarine groundwater discharge, *Geochimica and Cosmochimica Acta*, **62**, 3047-3054

Shim M-J., Swarzenski P. W. and Shiller A. M. (2012) Dissolved and colloidal trace elements in the Mississippi River delta outflow after Hurricanes Katrina and Rita, *Continental Shelf Research*, **42**, 1-9, doi:10.1016/j.csr.2012.03.007

Souza T. A., Godoy J. M., Godoy M. L. D. P., Moreira I., Carvalho Z. L., Salomão M. S. M. B. and Rezende C. E. (2010) Use of multitracers for the study of water mixing in the Paraiba do Sul River estuary, *Journal of Environmental Radioactivity*, **101**, 564-570, doi:10.1016/j.jenvrad.2009.11.001

Stecher H. A., and Kogut M. B. (1999) Rapid barium removal in the Delaware estuary, *Geochimica and Cosmochimica Acta*, **63**, 1003-1012

Swarzenski P. (2007) U/Th series radionuclides as coastal groundwater tracers, *Chem. Rev.*, **107**, 663-674, doi:10.1021/cr0503761

Swarzenski P., Campbell P., Porcelli D. and McKee B. (2004) The estuarine chemistry and isotope systematics of $^{234,238}U$ in the Amazon and Fly Rivers, *Continental Shelf Research*, **24**, 2357-2372, doi:10.1016/j.csr.2004.07.025

Tieman Z. G., Stewart B. W., Capo R. C., Phan T., Lopano C. and Hakala J. A. (2020) Barium isotopes track the source of dissolved solids in produced water from the unconventional Marcellus shale gas play, *Environmental Science and Technology,* **54,** 4275-4285, doi:10.1021/acs.est.0c00102

van Zuilen K., Nagler T. F. and Bullen T. D. (2016) Barium isotopic compositions of geological reference materials, *Geostandards and Geoanalytical Research*,**40**, 543-558, doi:10.1111/ggr.12122

van Maren D. S., Liew S. C. and Hasan G. M. J. (2014) The role of terrestrial sediment on turbidity near Singapore's coral reefs, *Continental Shelf Research,*, **76**, 75-88, doi:10.1016/j.csr.2013.12.001

Von Damm K. L., Edmond J. M., Grant B., Measures C. I., Walden B. and Weiss R. F. (1985) Chemistry of submarine hydrothermal solutions at 21°N, East Pacific Rise, *Geochimica and Cosmochimica Acta,* **49**, 2191-2220

Walter B. D. and Nims M., K. (2015) Spatiotemporal variation of trace elements and stable isotopes in subtropical estuaries: I. Freshwater endmembers and mixing curves, *Estuaries and Coasts,* **38**, 754-768, doi:10.1007/s12237-014-9881-7

Wolgemuth K., and Broecker W. S. (1970) Barium in sea water, *Earth and Planetary Science Letters*, **8**, 372-378

Zhang G-L., Pan J-H., Huang C-M. and Gong Z-T. (2007) Geochemical features of a soil chronosequence developed on basalt in Hainan Island, China, *Revista Mexicana de Ciencias Geologicas,* **24**, 261-269

Table 1, Dissolved Ba concentration and $\delta^{138/134}$Ba results for samples from the Amazon, Fly and Johor River estuaries.

Latitude °N	Longitude °E	Collection Date	Salinity	Ba concentration (nmol kg^{-1})		$\delta^{138/134}$Ba
				ICP-MS	TIMS	
Amazon River Estuary						
1.17417	49.09333	18/03/1996	0.32		123.6	0.15
2.90389	50.14167	07/03/1996	16.58	151.3	138.7	0.11
1.49417	47.90833	22/03/1996	16.31	192.9	194.7	0.04
4.58750	51.27000	08/03/1996	21.23	137.5	125.8	0.10
3.94389	50.60361	11/03/1996	24.80	123.4	111.3	0.13
3.96917	50.57889	12/03/1996	28.21	93.8	85.4	0.20
2.97417	49.11917	22/03/1996	32.73	59.7	55.2	0.44
9.01361	55.18722	24/03/1996	34.58	57.1	53.3	0.46
11.45944	57.88944	25/03/1996	35.65	48.7	48.0	0.49
6.86833	52.94389	23/03/1996	35.84	39.8	37.4	0.54
Fly River estuary						
-8.392	143.022		2	237	257.7	0.19
-8.383	143.117		4	237	509.2	0.13
-8.392	143.265		8	388	419.7	0.14
-8.359	143.352		10	368	411.8	0.12
-8.373	143.766		24	162	188.7	0.11
-8.781	143.985		35	43	62.5	0.33
Johor River estuary						
1.72662	103.89961	03/11/2017	0	368.6	351.5	0.19
1.69909	103.92558	03/11/2017	8	828.1	837.9	-0.02
1.68976	103.94888	03/11/2017	9	444.2	417.0	0.07
1.66540	103.93163	03/11/2017	15	383.0	381.6	0.09
1.63458	103.97203	03/11/2017	20	372.3	351.6	0.19
1.58442	103.98727	03/11/2017	25	252.4	260.7	0.15
1.42067	104.00174	17/12/2015	27	83.7	79.2	0.34
1.42050	104.00240	16/04/2016	27	107.7	96.3	0.21

Barium concentrations determined by inductively coupled plasma mass spectrometry (ICP MS) for the Fly River estuary are from Swarzenski et al. (2004). Uncertainty on $\delta^{138/134}$Ba is ± 0.03 ‰ based on long-term reproducibility (2sd) of the standard reference material NIST 3104a, with the exception of Amazon salinity 34.58 for which an uncertainty of ± 0.04 ‰ is assigned, representing the internal reproducibility of this analysis (2se).

Table 2, Estimates of the effective river Ba concentrations and $\delta^{138/134}$Ba values, and the amount and $\delta^{138/134}$Ba of dissolved Ba added by estuarine processes in the Amazon, Fly and Johor river estuaries.

	Amazon	**Fly**	**Johor**
$[Ba]_{river}$ (nmol kg^{-1})	124	143	352
$\delta^{138/134}Ba_{river}$ ‰	0.15 ± 0.03	0.34 ± 0.19	0.19 ± 0.03
$[Ba]_{effective}$ (nmol kg^{-1})	268 ± 46	512 ± 74	1039 ± 318
$\delta^{138/134}Ba_{effective}$ ‰	0.01 ± 0.06	0.11 ± 0.06	0.06 ± 0.12
$[Ba]_{added}$ (nmol kg^{-1})	144 ± 48	369 ± 76	688 ± 320
$\delta^{138/134}Ba_{added}$ ‰	-0.11 ± 0.13	0.02 ± 0.15	-0.01 ± 0.19
$\Delta^{138/134}Ba_{dissolved\text{-}adsorpted}$ ‰	-0.26 ± 0.14	-0.32 ± 0.28	-0.20 ± 0.19

$[Ba]_{river}$ and $\delta^{138/134}Ba_{river}$ denote the Ba concentration and $\delta^{138/134}$Ba value of the river dissolved load. $[Ba]_{effective}$ and $\delta^{138/134}Ba_{effective}$ denote the Ba concentration and $\delta^{138/134}$Ba value of the effective river endmembers, which represent the theoretical Ba concentration and $\delta^{138/134}$Ba value of a parcel of river water after modification by estuarine processes. $[Ba]_{added}$ and $\delta^{138/134}Ba_{added}$ denote the amount and isotope composition added to a parcel of river water by estuarine processes, calculated using equations 2 and 3. $\Delta^{138/134}Ba_{dissolved\text{-}adsorpted} = \delta^{138/134}Ba_{river} - \delta^{138/134}Ba_{added}$. Uncertainties on $[Ba]_{added}$, $\delta^{138/134}Ba_{added}$ and $\Delta^{138/134}Ba_{dissolved\text{-}adsorpted}$ were calculated by propagation of the uncertainties for $[Ba]_{river}$, $\delta^{138/134}Ba_{river}$, $[Ba]_{effective}$ and $\delta^{138/134}Ba_{effective}$ by Monte Carlo simulation (Supplementary Information). Note that for the Fly River, $\delta^{138/134}Ba_{river}$ and $\delta^{138/134}Ba_{added}$ are estimated using mass balance calculations based on values for the effective river endmember and data for the sample at salinity 2 (Supplementary Information).

926 **Table 3,** Literature compilation of Ba concentrations data for river dissolved loads
927 ($[Ba]_{river}$) and effective river endmembers ($[Ba]_{effective}$) used to estimate the global riverine
928 Ba flux to the oceans

River	Water discharge $km^3\ yr^{-1}$	Sediment discharge $Mt\ yr^{-1}$	$[Ba]_{river}$ $nmol\ kg^{-1}$	River Ba flux $Gmol\ yr^{-1}$	$[Ba]_{effective}$ $nmol\ kg^{-1}$	Effective Ba flux $Gmol\ yr^{-1}$
Amazon[1]	6300	1200	126	0.80	262	1.65
Congo[2]	1300	43	133	0.18	170	0.22
Ganges-Bramaputra[3]	1270	1060	157	0.20	376	0.48
Yangtze[4]	900	470	231	0.21	520	0.47
Paraná-Uruguay[5]	670	100	NA	NA	208	0.14
Yenisei[6]	620	4.1	76	0.047	63	0.039
Lena[6]	520	20	74	0.039	134	0.070
Mississippi[7]	490	210	467	0.23	607	0.30
Ob[6]	390	16	69	0.027	91	0.035
Mackenzie[8]	310	100	393	0.12	499	0.16
Pearl[9]	260	25	212	0.055	253	0.066
Fly[10]	180	110	143	0.026	512	0.092
Indigirka[6]	55	11	NA	NA	191	0.010
Chao Phraya[11]	30	3	274	8.2×10^{-3}	416	0.012
Paraiba do Sul[12]	28	4	225	6.3×10^{-3}	275	7.7×10^{-3}
Hudson[13]	15	0.2	276	4.1×10^{-3}	297	4.5×10^{-3}
Savannah[14]	11	1	130	1.4×10^{-3}	208	2.3×10^{-3}
Burdekin[15]	10	3	1175	0.012	650	6.5×10^{-3}
Delaware[16]	10	1	181	1.8×10^{-3}	229	2.3×10^{-3}
Pee Dee[17]	6.9	0.43	NA	NA	215	1.5×10^{-3}
Cape Fear[17]	6.5	0.29	NA	NA	336	2.4×10^{-3}
Fitzroy[15]	5.3	3	395	2.1×10^{-3}	572	3×10^{-3}
Humber[18]	4.6	0.19	213	1×10^{-3}	465	2.1×10^{-3}
St Johns[17]	2.9	0.27	NA	NA	133	3.2×10^{-4}
Johor[19]	2.4	0.45	352	1×10^{-3}	1039	3×10^{-3}
Peace[20]	1.5		50	7.5×10^{-5}	267	4×10^{-4}
Nueces[21]	0.72	0.71	1170	8.4×10^{-4}	1428	1×10^{-3}
Discharge weighted average			155		282	
Un-weighted average			287		387	

929 All water and sediment discharge values are taken from Milliman and Farnsworth (2011),
930 with the exception of sediment discharge of the Johor River (van Maren et al., 2004).
931 $[Ba]_{river}$ and $[Ba]_{effective}$ are based on estuarine Ba distributions from the following sources:
932 [1]This study and Boyle (1976), [2]Edmond et al. (1978), [3]Carroll et al. (1993), [4]Edmond et
933 al. (1985), [5]Hsieh and Henderson (2017), [6]Guay and Falkner (1998), [7]Hanor and Chan
934 (1977), Shim et al. (2012) and Joung and Shiller (2014), [8]Guay and Falkner (1998) and
935 Kipp et al. (2020), [9]Hong et al. (2018), [10]Swarzenski et al. (2004) and this study, [11]Nozaki
936 et al. (2001), [12]Souza et al., (2010), [13] Li and Chan, (1979), [14]Shaw et al. (1998) and
937 Moore and Shaw (2008), [15]Lewis et al. (2018), [16]Coffey et al. (1997) and Stecher and
938 Kogut (1999), [17]Moore and Shaw (2008), [18]Coffey et al., (1997), [19]this study, [20]Frolich et
939 al. (1985), [21]Walter and Nims (2015). NA- not available.

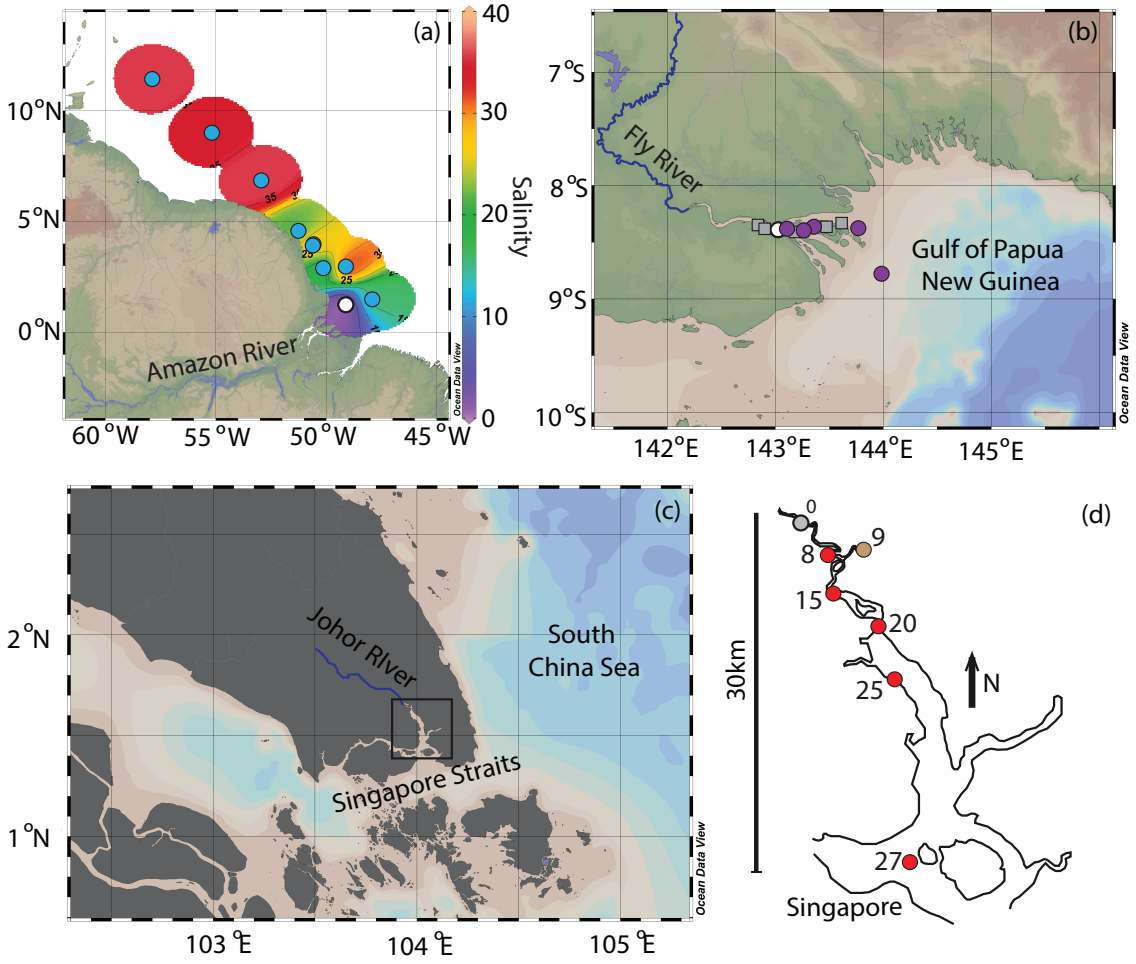

940

941 **Figure 1,** Locations of samples from the Amazon, Fly and Johor River estuaries. Panel (a)
942 and (b) display locations of samples from the Amazon freshwater plume, and the Fly
943 River estuaries respectively (Swarzenski et al., 2004). In panel (b) the purple and open
944 circles denote samples analyzed in this study for Ba concentrations and isotope
945 compositions, while the grey squares denote samples measured for Ba concentrations only
946 by Swarzenski et al. (2004). Panels (c) and (d) display the location of the Johor River
947 estuary, and sampling locations (circles) within the Johor River estuary respectively
948 (Chen et al., 2015). In panel (d), the grey, brown and red circle(s) denote the sampling
949 locations of Johor River water, a separate tributary, and estuarine waters respectively, and
950 the numbers denote the salinities at the different sampling locations.

951

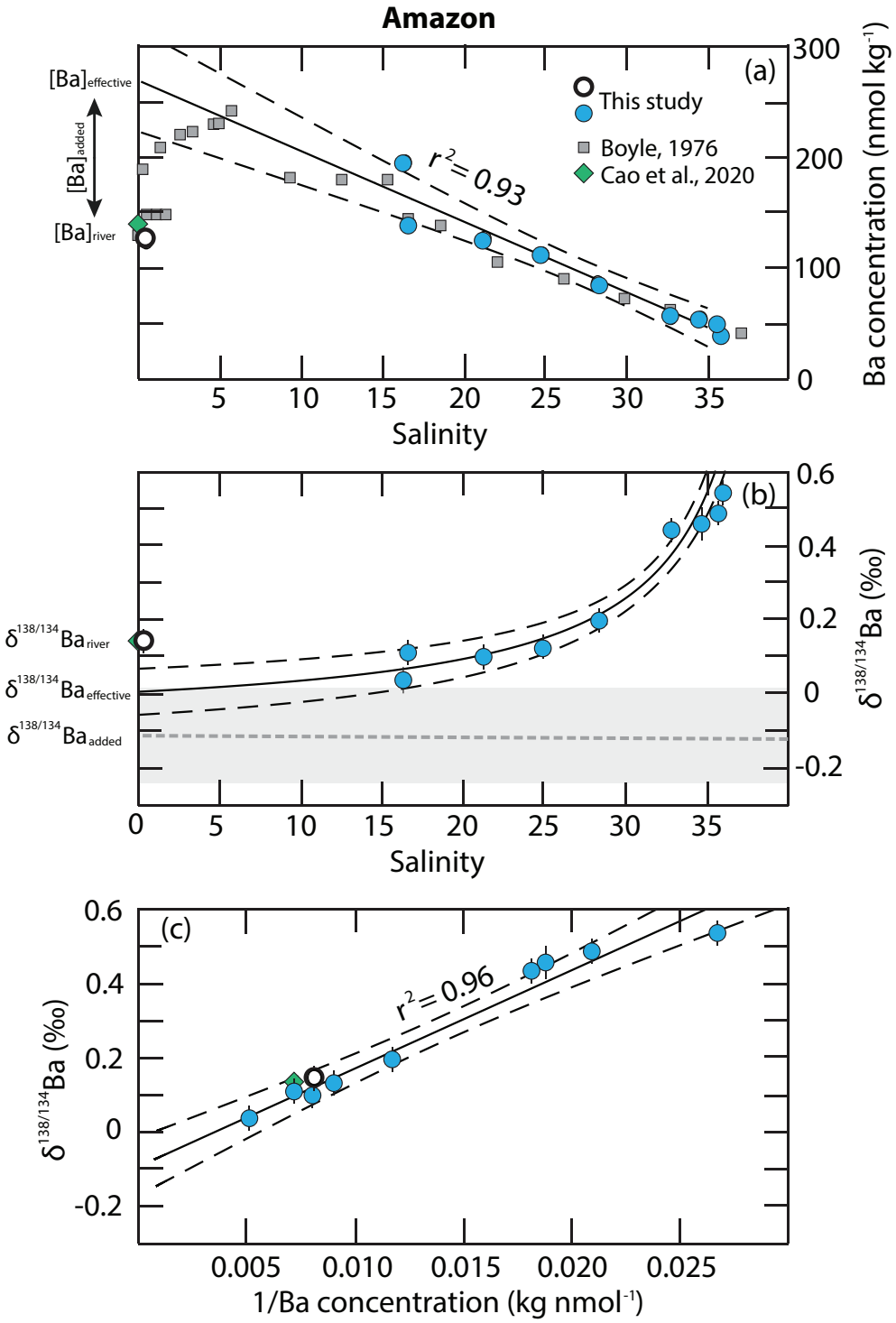

952

953 **Figure 2**, Relationships between salinity, Ba concentrations and $\delta^{138/134}$Ba values in the

954 Amazon River estuary. Solid black lines represent conservative mixing relationships,

955 defined by linear regressions between Ba concentration and salinity (panel a) and

956 $\delta^{138/134}$Ba and 1/Ba concentration (panel c) with dashed lines showing 95% confidence

957 intervals. The mixing relationship in panel (b) is defined by combining the linear

958 regressions in panels (a) and (c). Open circle denotes the Amazon River water
959 endmember, which is omitted from regressions to define mixing relationships. Literature
960 data are displayed by grey squares (Boyle, 1976) and the green diamond (Cao et al.,
961 2020). In panel (b) the horizontal grey dashed lines show the $\delta^{138/134}$Ba value estimated
962 for the Ba added to the dissolved riverine flux by estuarine processes, with uncertainties
963 shown by the grey shaded intervals.
964
965

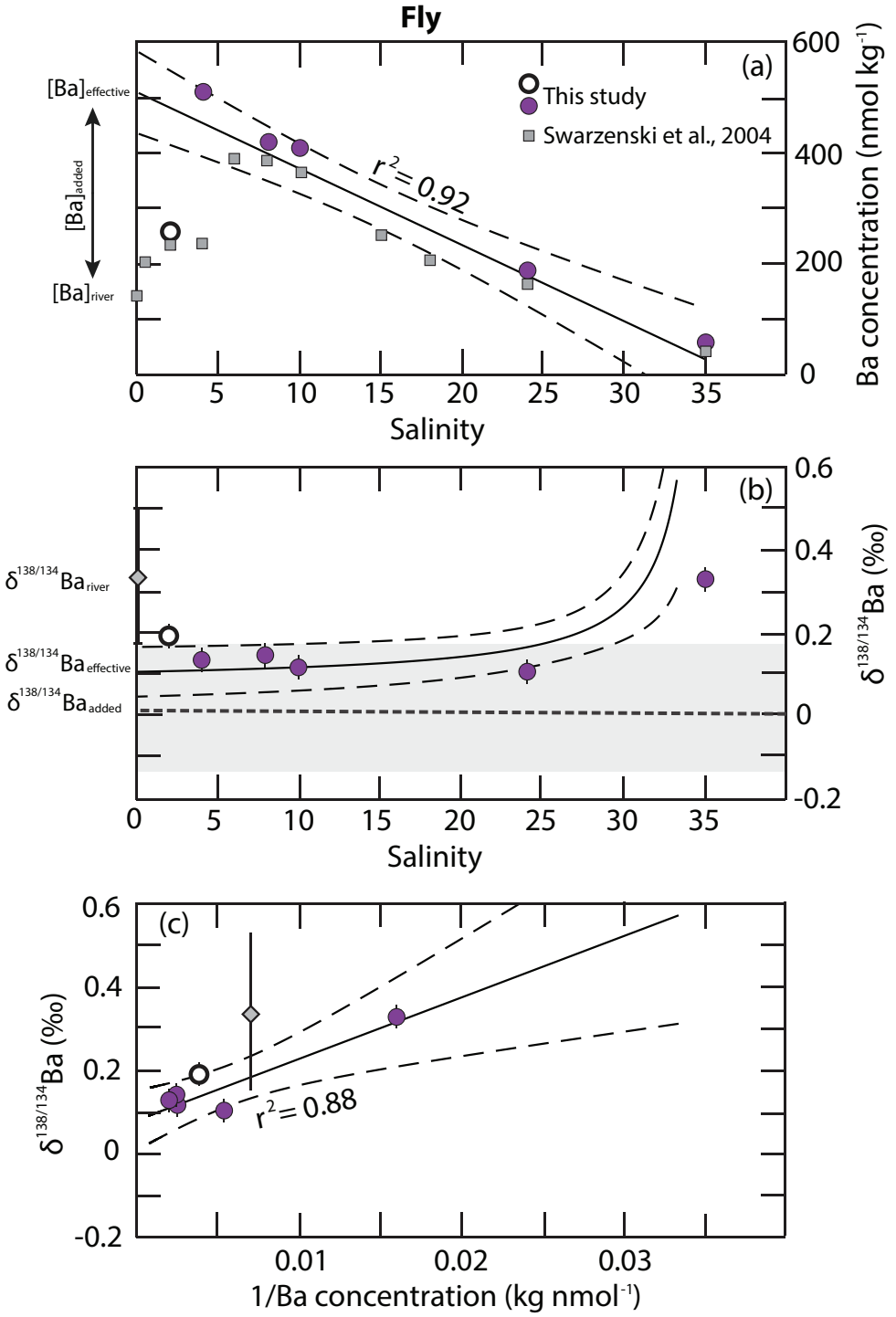

966

967 **Figure 3**, Relationships between salinity, Ba concentrations and $\delta^{138/134}$Ba values in the
968 Fly River estuary. Solid black lines represent conservative mixing relationships, defined
969 by linear regressions between Ba concentration and salinity (panel a) and $\delta^{138/134}$Ba and
970 1/Ba concentration (panel c) with dashed lines showing 95% confidence intervals. The
971 mixing relationship in panel (b) is defined by combining the linear regressions in panels

(a) and (c). Open circle denotes the sample at salinity 2, which is omitted from regressions to define mixing relationships. Grey squares display previously published Ba concentration data for these samples (Swarzenski et al., 2004). The grey diamond denotes the $\delta^{138/134}$Ba value estimated for the Fly River dissolved load (Supplementary Information). In panel (b) the horizontal grey dashed lines show the $\delta^{138/134}$Ba value estimated for the Ba added to the dissolved riverine flux by estuarine processes, with uncertainties shown by the grey shaded intervals.

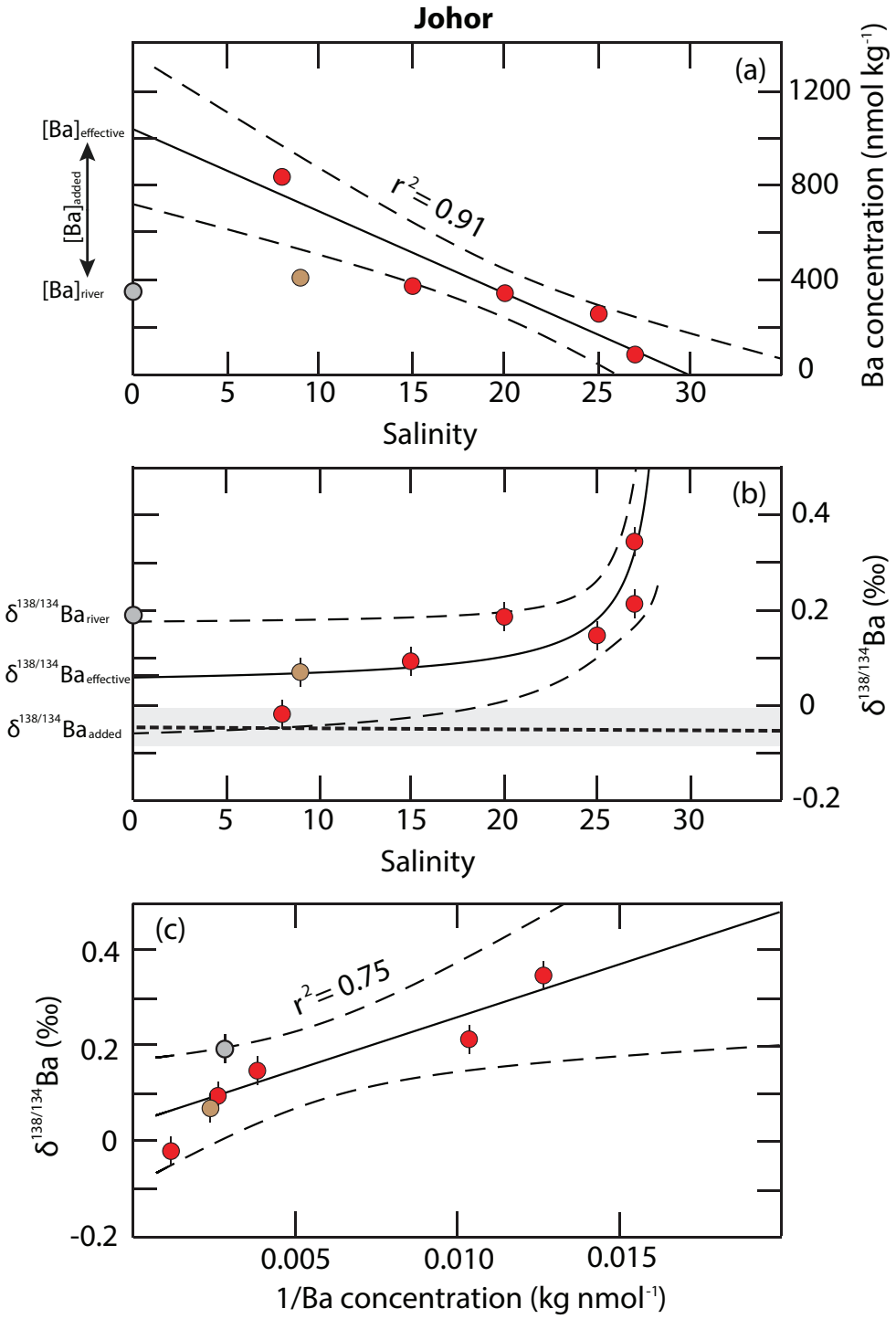

980

981 **Figure 4**, Relationships between salinity, Ba concentrations and $\delta^{138/134}$Ba values in the

982 Johor River estuary. Solid black lines represent conservative mixing relationships, defined

983 by linear regressions between Ba concentration and salinity (panel a) and $\delta^{138/134}$Ba and

984 1/Ba concentration (panel c) with dashed lines showing 95% confidence intervals. The

985 mixing relationship in panel (b) is defined by combining the linear regressions in panels

(a) and (c). The grey circle and brown circle denote the Johor River endmember and a sample from the separate tributary to the Johor estuary, which are omitted from regressions to define the mixing relationships. In panel (b) the horizontal grey dashed lines show the $\delta^{138/134}$Ba value estimated for the Ba added to the dissolved riverine flux by estuarine processes, with uncertainties shown by the grey shaded intervals.

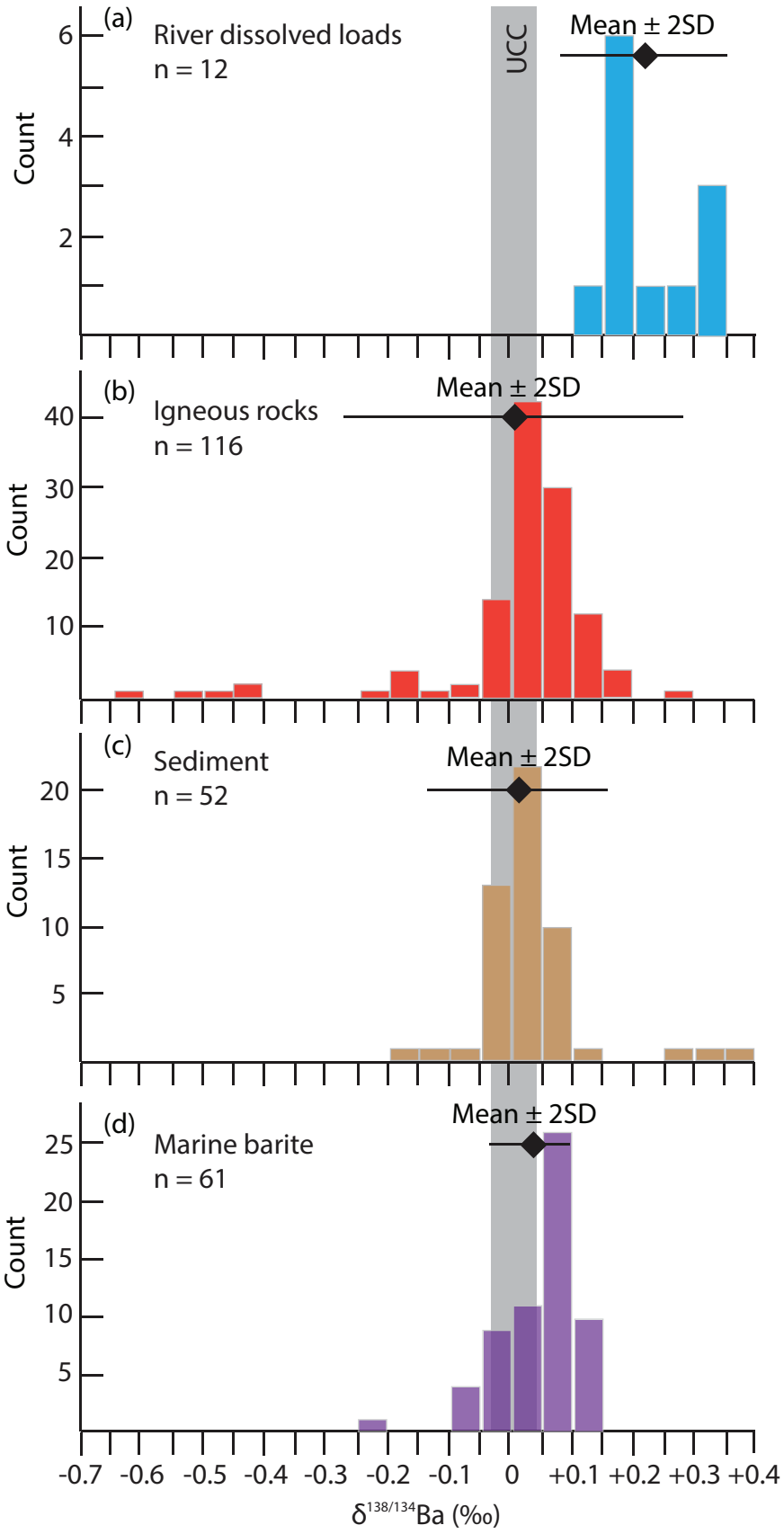

992

993 **Figure 5,** Histograms of the $\delta^{138/134}$Ba of river dissolved loads, igneous and sedimentary

994 rocks, and marine barite. River dissolved load data for the rivers Yangtze, Amazon,

995 Yukon, Pearl, Sepik, Danube, Lena, Colorado, Ohio, Yellow, Fly and Johor are from Gou
996 et al. (2020), Cao et al. (2020), Tieman et al. (2020) and this study. For the Yellow River
997 timeseries $\delta^{138/134}$Ba measurements are available (Gou et al., 2020), and the Ba flux
998 weighted average $\delta^{138/134}$Ba of 0.28 ‰ is used. Igneous and sedimentary rock data are
999 from Miyazaki et al. (2014), Nan et al. (2015), van Zuilen et al. (2016), Bullen and
1000 Chadwick (2016,) Bridgestock et al. (2018), Nielsen et al. (2018), Nan et al. (2018),
1001 Nielsen et al., (2020), An et al. (2020) and Lin et al. (2020). Data for marine $BaSO_4$ are
1002 from Crockford et al. (2019). The grey bar represents the average composition of the
1003 upper continental crust (UCC) given by Nan et al. (2018).
1004

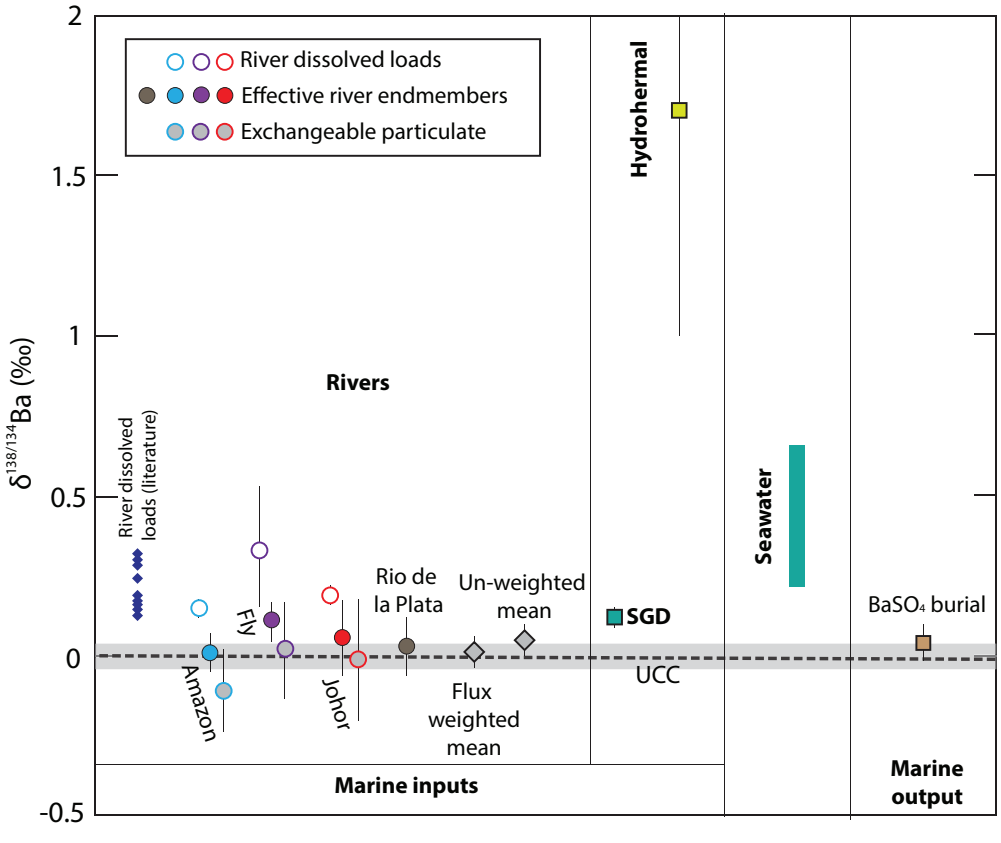

1005

1006 **Figure 6,** Constraints on the marine Ba isotope budget. Grey diamonds display the Ba
1007 flux weighted and un-weighted mean of effective river $\delta^{138/134}$Ba values, representing net
1008 riverine inputs to the ocean. The horizontal dashed line and grey shaded area shows the

1009 $\delta^{138/134}$Ba of the upper continental crust (UCC; Nan et al., 2018). Blue diamonds display
1010 literature data for dissolved loads of the Yangtze, Amazon, Yukon, Pearl, Sepik, Danube,
1011 Lena, Coloarado, Ohio and Yellow Rivers (Gou et al., 2020, Cao et al., 2020, Tieman et
1012 al., 2020). The effective river $\delta^{138/134}$Ba of the Rio de la Plata estuary is from Hsieh and
1013 Henderson (2017). Constraints on the average $\delta^{138/134}$Ba of freshwater submarine
1014 groundwater (SGD) and hydrothermal inputs (following modification by BaSO4
1015 precipitation) are from Mayfield et al. (2021) and Hsieh et al. (2021) respectively.
1016 Seawater data are from Horner et al. (2015), Bates et al. (2017), Hsieh and Henderson
1017 (2017), Bridgestock et al. (2018), Hemsing et al. (2018) and Geymann et al. (2019). The
1018 average $\delta^{138/134}$Ba of modern marine barite (± 2sd) is from Crockford et al (2019).
1019

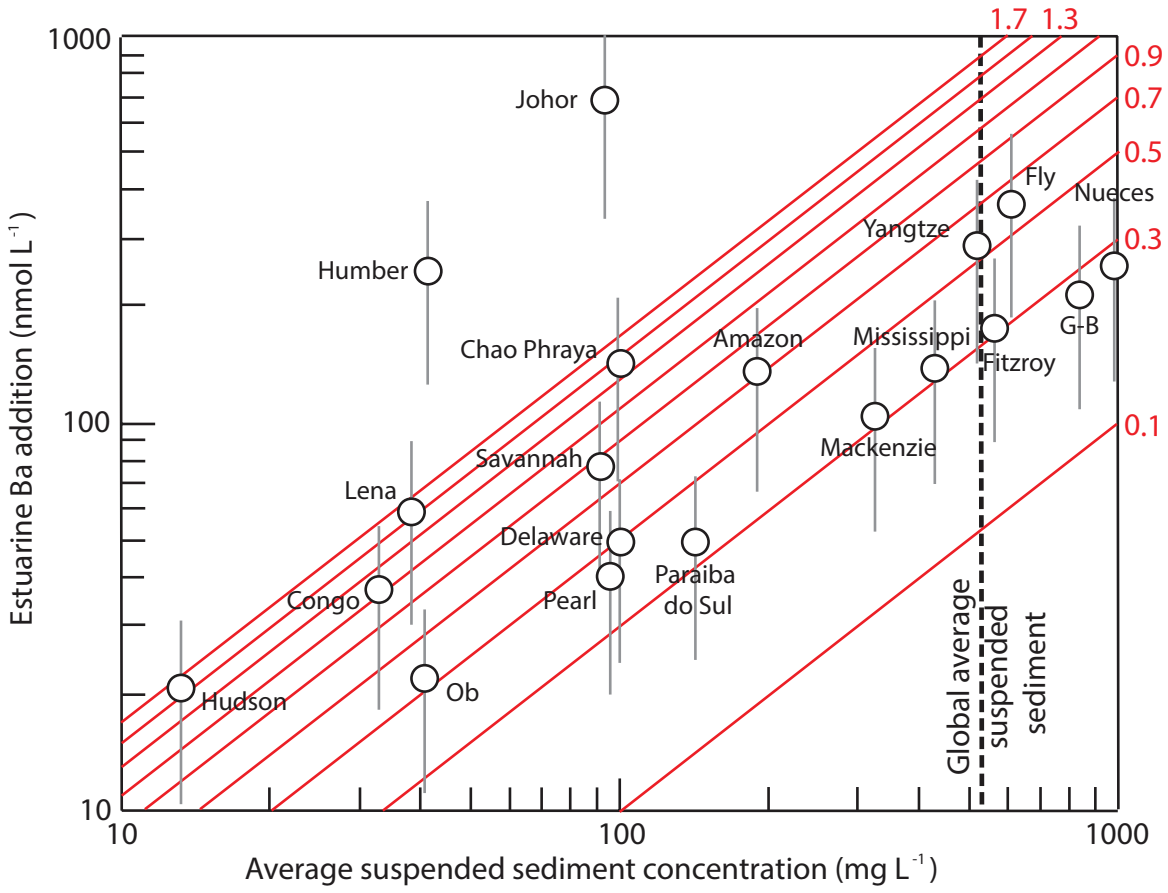

1020

1021 **Figure 7**, Magnitude of estuarine Ba addition ($[Ba]_{added}$) versus annual average suspended
1022 sediment concentrations for global rivers. $[Ba]_{added}$ is calculated following eqn. 2 from

estuarine Ba distributions compiled from published literature (Table 3, Supplementary Information, Electronic Data). For rivers for which multiple estuarine Ba distributions exist, averaged $[Ba]_{river}$ and $[Ba]_{effective}$ are used to calculated $[Ba]_{added}$. A conservative relative uncertainty of ± 50 % is assigned to $[Ba]_{added}$ to reflect the potential scale of temporal variations in $[Ba]_{river}$ and $[Ba]_{effective}$ for individual rivers (Supplementary Information). Red contours show Ba release per mass of sediment (nmol mg^{-1}), and span the range of measured exchangeable Ba concentrations for riverine suspended sediments (0.12 to 1.7 nmol mg^{-1}; Li and Chan, 1979, Coffey et al., 1997, Samanta and Dalai, 2016, Gou et al., 2020). Annual average suspended concentrations are from Milliman and Farnsworth (2011). The dashed vertical line shows the average global river suspended sediment concentration, of 528 mg L^{-1} (Milliman and Farnsworth, 2011). G-B denotes the Ganges-Brahmaputra river system. Rivers for which constraints on $[Ba]_{river}$ are not available in the compiled literature estuarine Ba distributions are not included in this figure. The rivers Burdekin and Yenisey display negative $[Ba]_{added}$ values and are not included in this plot, nor is the Peace River due to lack of suspended sediment data.